*Geophys. J. Int.* (1993) **115,** 759–777

# Earthquake location in strongly heterogeneous media

G. Wittlinger, G. Herquel and T. Nakache
*Institut de Physique du Globe, 5 rue René Descartes, F-67084 Strasbourg Cedex, France*

Accepted 1993 April 5. Received 1993 March 30; in original form 1992 December 21

## SUMMARY

Traveltime computation methods for strongly heterogeneous 3-D media developed during recent years are well suited for earthquake location. We present here a new method based on the traveltime algorithm of Podvin–Lecomte, related to the inverse problem formulation of Tarantola & Valette. The Podvin–Lecomte method, based on the Huygens principle, is very robust and allows arbitrary surface topography and station placement even for borehole instruments. First arrival traveltimes are computed for each of the recording stations using a fine 3-D velocity mesh (up to $10^6$ cells on a workstation). The traveltime grid allows the use of the Tarantola & Valette formulation, which enables a full non-linear approach. The solution is given as a 3-D probability density function of hypocentre coordinates, which accounts for the arrival time measurements as well as *a priori* information for the location, the accuracy of both the arrival time readings and the computation of the theoretical traveltimes. This powerful method called 3DGRIDLOC gives the location of the induced seismicity of the gas field of Lacq (France) using 443 520 cells of a 3-D velocity mesh and the observations from nine recording stations, one of which is located at the bottom of a 3880 m deep borehole. Location of synthetic foci as well as more than 500 actual earthquakes shows the real advantages of this new method versus the classical HYPO71. A new insight into the induced seismicity is now possible: induced seismicity may occur as far away as 10 km from the gas reservoir and involve a much greater volume of rock than expected using earlier locations.

**Key words:** complex 3-D models, earthquake location, probability function.

## 1 INTRODUCTION

Most earthquake location models are derived from Geiger's method (1912). For local seismicity, where detailed and complex velocity models best account for the crustal heterogeneities, HYPO71 (Lee & Lahr 1975) is still the most popular method, even though only horizontal flat-layered velocity models can be used. Since most earthquakes do not occur in flat-layered areas it is important to use new location methods that incorporate complex 3-D velocity structures, as have been observed for subduction zones, volcanoes, and hydrocarbon fields.

Earthquake location is one of the classical **inverse problems** in geophysics, and it is, therefore, not surprising that several inverse methods have already been tested on hypocentral localization (Tarantola & Valette 1982; Hirata & Matsu'ura 1987). The earthquake location problem can generally be split into two main stages: (1) the forward problem, dealing with the computation of the theoretical traveltimes; (2) the inverse problem, dealing with the search for the unknown parameters of the hypocentres. Generally speaking, the forward problem is much more difficult to solve than the inverse one, and earthquake location techniques are not an exception to this rule. The basic difficulty in running more accurate earthquake location methods, lies in the difficulty of computing the theoretical traveltimes in strongly heterogeneous media.

As one generally uses first arrival times for earthquake localization methods, finite difference methods for solving the eikonal equation (Vidale 1988, 1990), or Huygens' principle (Podvin & Lecomte 1991) (PL method hereafter) or shortest path methods (Moser 1991) seem to be well adapted for theoretical arrival time computations.

Earthquake location is basically a strongly non-linear inverse problem, and therefore the location methods are usually linearized, and solved with an iterative scheme. As a consequence, instability problems may appear due to strong variations of the partial derivatives. Moreover, only focal parameters lying in the vicinity of the trial solution are retrieved. As we generally have no precise knowledge of the

actual location, a method such as that of Tarantola & Valette (1982), searching for the hypocentre in the whole medium, would seem to be preferable.

In this paper we will focus on the combination of these two concepts: a grid computation of traveltimes for the forward problem and the computation of the *a posteriori* probability density function in order to obtain a powerful location tool called 3DGRIDLOC. A similar scheme was developed by Moser, Van Eck & Nolet (1992) using a shortest path traveltime computation method. Nelson & Vidale (1990) used a related method for computing the traveltimes, but a very different formulation for the inverse problem. The contribution of this paper lies in the two following ideas: (1) the combination of two powerful methods; (2) the application to the location of gas-extraction-induced seismicity in a well-known complex geological structure.

## 2 THE LOCATION METHOD

### 2.1 The forward problem

This constitutes the computation of theoretical traveltimes. The velocity model is described by a 3-D mesh of regular cubic cells. In each cell the velocity is specified. For each recording station the computed traveltime grid using the reciprocity principle, for sources located in each cell, gives the traveltime of the first arrival. This computation may be carried out using any grid ray tracing method. After some performance tests (Lecomte 1992) we chose the PL method instead of Vidale's method for its better robustness. Difficulties may arise when using such a grid method in models with very sharp contrasts, where the first arrivals may be diffracted waves. These waves generally have very little energy and are thus difficult to detect on actual records. In order to suppress most of these low-energy diffracted waves we applied a smoothing algorithm to the velocity model. Traveltimes do not change much between smoothing models but grid methods are more accurate.

The computations take interpolation into account since in real networks recording stations are not located exactly on grid nodes. There is no limitation in accounting for the exact station elevation and surface topography, which is important in mountainous areas or, as shown in our illustrative example, for sensors located in boreholes.

Moreover if shear waves are observed at some stations, by assuming a constant Poisson's ratio for the whole medium, the $S$-wave time-grids can simply be deduced from the $P$-wave grids. If Poisson's ratio is not constant, new traveltime grids must be computed for the $S$-waves.

### 2.2 The inverse problem

This constitutes the search for the focal parameters. As a basic assumption we postulate that all the first arrival rays are contained within the 3-D mesh. If this is not the case we have to enlarge the 3-D mesh to fulfil this condition.

After computing the traveltime grids, we are faced with a very unusual but propitious situation in inverse problems. To obtain the solution of the inverse problem it is necessary to decide which cell among the grid cells will contain the hypocentre. Under the constraint of having a good fit to the actual arrival time measurements, we have several options: for instance, we can use the mean square traveltime residual ($L_2$ norm) or the mean absolute value of traveltime residual ($L_1$ norm). However, the Tarantola & Valette (1982) formulation using a probability density function is easy to apply and provides a powerful tool to assess the possible hypocentres.

In particular, *a priori* information on hypocentre location may be incorporated. Errors on both observed and theoretical traveltimes can be used with probability laws that are not necessarily Gaussian.

Tarantola & Valette (1982) shows that assuming Gaussian probability laws for both observations and the theoretical relationship, the integration over time of the probability density function may be performed analytically. This means that in this case there is no need to use time sampling to search for the origin time, thus saving a lot of computation time. If the origin time is really needed it can be obtained as a weighted average of the observed arrival times minus the weighted computed traveltimes (Nelson & Vidale 1990; Moser *et al.* 1992).

The basic relationship used to evaluate the spatial probability density function (PdF) of the hypocentre is relation (10-8) of Tarantola & Valette (1982):

$$\sigma(X, Y, Z) = K\rho(X, Y, Z) \times \exp\{-\tfrac{1}{2}[\mathbf{t}_0 - \mathbf{h}(X, Y, Z)]^{\mathrm{T}}(\mathbf{C}_t + \mathbf{C}_T)^{-1}[\mathbf{t}_0 - \mathbf{h}(X, Y, Z)]\}, \quad (1)$$

where $K$ is a normalization factor introduced when integrating over time, which may depend on the spatial coordinates $X,Y,Z$; $\rho(X, Y, Z)$ is an arbitrary *a priori* PdF containing all the *a priori* information that we have on the parameters (this is a convenient way to constrain the location of the hypocentres in certain key areas and to rule out locations which are too shallow or too deep); $\mathbf{t}_0$ is the vector of observed arrival times minus the mean of observed arrival times at the recording stations; $\mathbf{h}(X, Y, Z)$ is the vector of the theoretical traveltimes minus the mean of theoretical traveltimes; $\mathbf{C}_t$ and $\mathbf{C}_T$ are the variance–covariance matrices of both the observations and the theoretical relationship. As noted by Tarantola & Valette (1982) $\mathbf{C}_t + \mathbf{C}_T$ acts as a sum matrix, as a result of the Gaussian probability laws.

Straightforward computation gives then the marginal PdF of the horizontal $X,Y$ and vertical $Z$ coordinates:

$$\sigma(X, Y) = \int_Z \sigma(X, Y, Z)\, dZ, \qquad \sigma(Z) = \iint_{XY} \sigma(X, Y, Z)\, dX\, dY. \quad (2)$$

From these marginal PdF we obtain the coordinates of the hypocentre using, either the absolute maxima, or the expected value. The confidence region is not necessarily ellipsoidal as shown in the following section, but an approximation of the location error is given after determination of the principal axes of the error ellipsoid using the variances–covariances matrix of the three focal parameters. The best way to appreciate the confidence region is to look at the shape of the three marginal PdF

$\sigma(X, Y)$, $\sigma(X, Z)$ and $\sigma(Y, Z)$.

$$E(X) = \int \sigma(X) X\, dX \qquad \mathrm{Var}\,(X) = \int [X - E(X)]^2 \sigma(X)\, dX,$$

$$E(Y) = \int \sigma(Y) Y\, dY \qquad \mathrm{Var}\,(Y) = \int [Y - E(Y)]^2 \sigma(Y)\, dY,$$

$$E(Z) = \int \sigma(Z) Z\, dZ \qquad \mathrm{Var}\,(Z) = \int [Z - E(Z)]^2 \sigma(Z)\, dZ. \tag{3}$$

### 2.3 How to save computation time

For dense velocity grids of about $10^6$ cells, the computation of the traveltime grids becomes time consuming especially in the case of many recording stations, although these computations have to be carried out only once. The search for the hypocentre location amongst all the cells of the grid must be done for each earthquake. To reduce the computation time required for this stage, an alternative method based on a two-scale process can be used (Nelson & Vidale 1990). The original fine traveltime grids are resampled, and eqs (1) and (2) are then computed using an adapted covariance matrix $\mathbf{C}_T$ in order to obtain a rough location. In the vicinity of this first location we use the initial fine traveltime grid to search for the final hypocentre location obtained with the precision of the initial cell dimension. If there is a need for an even more precise location, finer than the initial mesh, then we interpolate the original traveltime grids in the vicinity of the last location cell and apply eqs (1) and (2) to the locally oversampled grids.

## 3 A SYNTHETIC DATA TEST

### 3.1 The velocity model and the traveltimes grids

As there is no advantage in applying this method to homogeneous half-spaces or plane-layered media, we performed our test for a more complex structure where HYPO71 is apparently inefficient. In order to mimic a realistic situation, we used the actual velocity model describing the anticlinal structure of the Lacq gas field (France). Since 1974 the induced seismicity of this gas field has been monitored by a telemetered network (Wittlinger 1980; Grasso & Wittlinger 1990). The velocity model that we used has been established by Guyoton, Grasso & Volant (1992) on the basis of lithological borehole data and seismic reflection profiles. We re-sampled the original cubic cells of the velocity model in order to obtain regular equidimensional cells with sides of 250 m. As actual hypocentre locations may be deeper than the bottom of the original model, we enlarged the velocity mesh in depth using a small positive velocity gradient. The final model consisted of $88 \times 72 \times 70$ cubic cells defining a cubic volume of 22 km in a north–south direction, 18 km in a east–west direction and down to 17.5 km in depth. Two features of this model are of importance for hypocentral location: (1) a north–south asymmetric anticlinal structure; (2) the existence of numerous low- and high-velocity zones. A glance at this model (Figs 1a and b) shows that extracting a flat-layered model from this more realistic one would clearly be an oversimplification. Velocities vary from 2.7 km s$^{-1}$ for the thick superficial layer to 6.4 km s$^{-1}$ at the bottom of the model. Velocities as high as 6.1 km s$^{-1}$ also appear in some superficial zones of the Recifal formation. We can also see that the seal of the gas reservoir created by the Sainte Suzanne marls is the main low-velocity zone of this structure.

Figures 2(a) and (b) show cross-sections of the traveltime grids for a surface station (LDB) and for the downhole seismometer (PRO). Obviously, due to the low- and high-velocity zones the wavefronts are no longer spherical or regular. This can also be seen in Figs 3(a) and (b) showing a selection of rays for station PRO.

Velocity perturbations due to strong anisotropy may reach 10 per cent or more in sedimentary rocks (Babuska & Cara 1991), which is typically of the same order of magnitude as the fine 3-D velocity variations modelled. Although traveltime grids can be computed using the PL method in 2-D anisotropic media (Lecomte 1993) extension to 3-D anisotropic media is not straightforward. Owing to the lack of information on anisotropy in this gas field and to the computational difficulties, we have not tried to account for anisotropy.

### 3.2 Performance tests

To compare the performance of 3DGRIDLOC with that of the classical HYPO71 algorithm, we have to build a layered velocity model from the actual 3-D model. The best way to do this is to average the velocities in each 250 m thick horizontal layer, thus obtaining the velocity–depth profile shown in Fig. 4(a). From this depth profile we construct a flat-layered model made of 12 layers (Fig. 4b). Fortunately, no low-velocity layer appears on this model, making it possible to use HYPO71.

The test consists of the localization of 144 synthetic foci, located along nine vertical lineaments as in Fig. 5. The synthetic arrival times with a random error of $\pm 0.02$ s added are computed using the PL method. The location of hypocentres is performed using both HYPO71 and 3DGRIDLOC.

Using HYPO71 (Figs 5a and b) neither the horizontal location nor the depth of the foci are correctly retrieved, except for the central lineaments of the foci located near the array centre of the network, for which the horizontal coordinates are well retrieved. Localization using this flat-layered model without any station correction leads to a clustering of all the hypocentres beneath the area covered by the recording stations. This clustering effect should be kept in mind when interpreting actual locations obtained using HYPO71. Considering the small size of the area investigated, very large differences, of up to 4 km for horizontal coordinates and 6 km for depth between computed and actual foci appear using HYPO71. We have not been able to find a layered velocity model giving an acceptable depth location for all the synthetic foci. Whichever velocity model we use, HYPO71 results, for most of the tested foci in 'good' hypocentres, in terms of rms time and the final standard error, but which may be quite distant from the real ones, especially in depth. This inadequacy of the layered velocity models becomes more and more

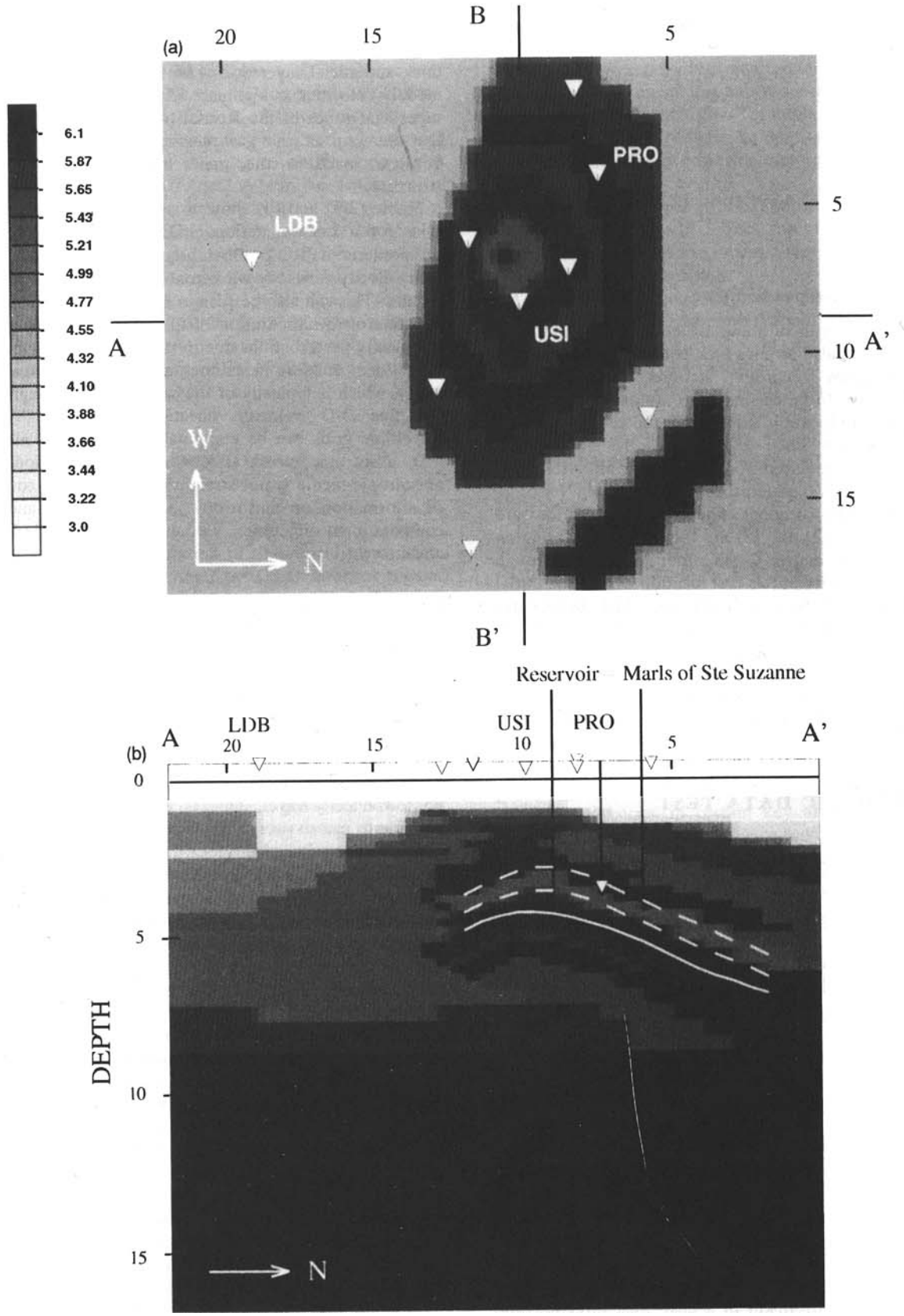


**Figure 1.** (a) Map view of the *P*-velocity model at 4.75 km depth, corresponding to the mean depth of the gas reservoir. Recording stations are projected on this map view. Distances are given in kilometres. (b) Vertical north–south cross-section (A–A'), with recording stations. In our example the station elevations vary from 0.09 to 0.255 km for the eight surface stations. The borehole seismometer is located in an unused well at 3880 m below sea-level.

*P*-wave velocities on the grey scale are in kilometres per second. Below 9 km we use a quite homogeneous velocity model with only a small vertical gradient of $+0.043\ \mathrm{km\,s^{-1}\,km^{-1}}$. Note the asymmetric anticlinal structure on the north–south cross-section as well as the low-velocity zone of the marls of Sainte Suzanne (Aptian, $V_P = 4.4\ \mathrm{km\,s^{-1}}$) and the reservoir (Portlandian–Barremian $V_P = 5.7$–$6.0\ \mathrm{km\,s^{-1}}$).

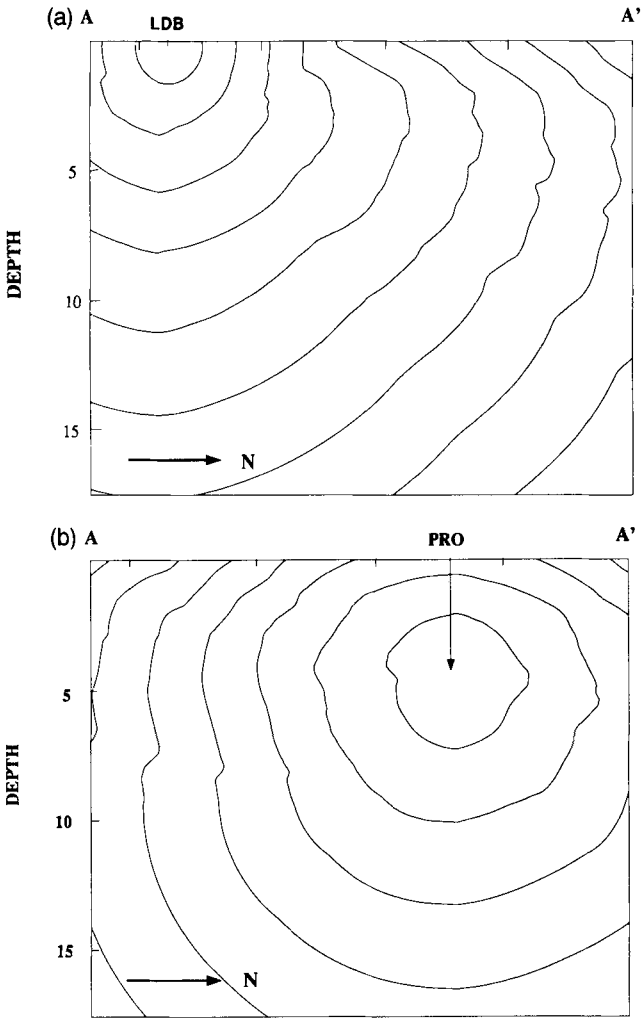


**Figure 2.** Vertical cross-section (north–south) of the traveltime grid showing the wavefronts starting at station LDB (a) and at station PRO, which is the borehole seismometer located at 3880 m depth (b). Wavefronts are plotted for every 0.5 s. These figures illustrate the reciprocity principle (exchange of source and station) used to compute the traveltimes in one step.

important when we reduce the number of recording stations. This was the situation at the beginning of the monitoring period in 1974–75 when the network was still in its early stages.

The failure of HYPO71 locations in these synthetic tests reflects only the fact that the complex velocity model of Lacq gas field cannot be reduced to a flat-layered model. We would probably have the same difficulties in subduction zones or other complex geological situations.

When inverting synthetic data with 3DGRIDLOC, the covariance matrix of the computed traveltimes reduces to intrinsic computation errors due to the PL method since there is no error in the velocity model. These computation errors are estimated to be less than $0.01\,s^{-1}$ using the flat-layered model where exact computations are feasible. The coordinates of the foci are determined here with either the absolute maxima of the marginal PdF or the expected value. If the shape of the PdF is symmetrical, there are no systematic differences between these two methods. For foci located near the borders of the model, the complete PdF is not available because of the truncation at the borders. In this case the expected value is biased and cannot give a correct estimation of the location. For this reason we use the determination corresponding to the absolute maxima of the PdF. It should be noted that the variance suffers the same bias, and is not suitable for an error estimation.

The locations obtained using 3DGRIDLOC (Figs 5c and d) are apparently more accurate than those obtained from HYPO71. Only a few foci located on the peripheral lineaments have location errors greater than 1 km. But this test also emphasizes that, for actual data, when the velocity model we use is no longer exactly the real one, it is unrealistic to refine the locations too much. In the case of our example, where we have chosen a 250 m cell length 3-D grid, it is meaningless because of the 0.02 s noise added and the 0.01 s computation error, to calculate locations more accurate than the cell dimension, which is equal to half of the dominant wavelength of these local earthquakes.

An earthquake location method should be robust and somewhat insensitive to weak velocity variations. We perform a robustness test using the same synthetics as in the previous test but adding a large $\pm 0.3$ s perturbation at one of the eight stations for each event. Such a time error is more than 10 times the realistic reading error (see below) and may be considered as a mistake. Figs 6(a) and (b) show horizontal and vertical north–south cross-sections obtained from these noisy synthetic data. For the epicentres located inside the station network, we retrieve the general pattern of the synthetic seismicity. For foci located outside of the network, such an error in the data set can strongly affect the locations.

We also examined the sensitivity of 3DGRIDLOC to small errors in the velocity model. The theoretical arrival time grids are now computed using a weakly perturbed velocity model obtained by adding or subtracting a $0.15\,km\,s^{-1}$ velocity perturbation to the geological formations with velocity varying from 4.0 to $6.2\,km\,s^{-1}$. This perturbation leads to traveltime differences up to 0.1 s. Such velocity variations are probably the upper bound of the velocity estimation error carried out when building up the velocity model of the Lacq gas field. The locations determined using this perturbed model are close to the locations found with the unperturbed model. Only some deep and off-centred foci present systematic errors (Figs 6c and d).

These tests on synthetic data lead to three main conclusions.

(1) The synthetic foci are retrieved with a good precision (mean rms times less than 0.006 s and mean mislocation distance less than 0.10 km), for the whole focal depth range and even for foci located outside the recording network.

(2) 3DGRIDLOC is at least as robust as HYPO71 with respect to large time errors and some mistakes in the data do not preclude acceptable locations.

(3) 3DGRIDLOC is not very sensitive to weak velocity perturbations in the model. This ensures that it provides reliable seismicity patterns even when the velocity model used is not perfect.

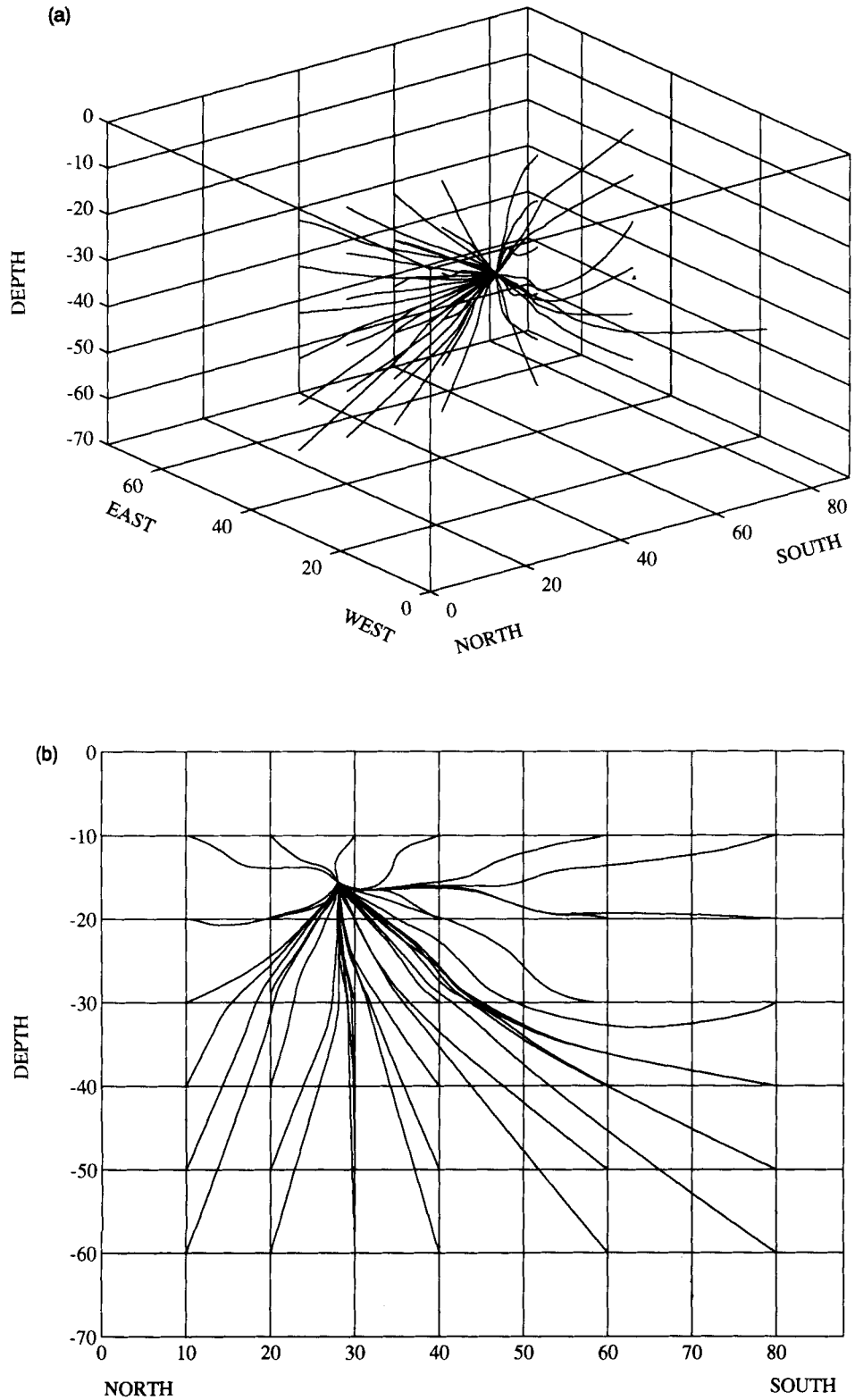


**Figure 3.** (a) Some ray paths in three dimensions starting at hypothetical hypocentres and ending at station PRO at 3880 m depth. This view is taken from the NW towards the SE, and the dimensions on the axes are given in number of cells with sides of length 0.250 km. (b) The same rays projected on a vertical north–south cross-section through the station.

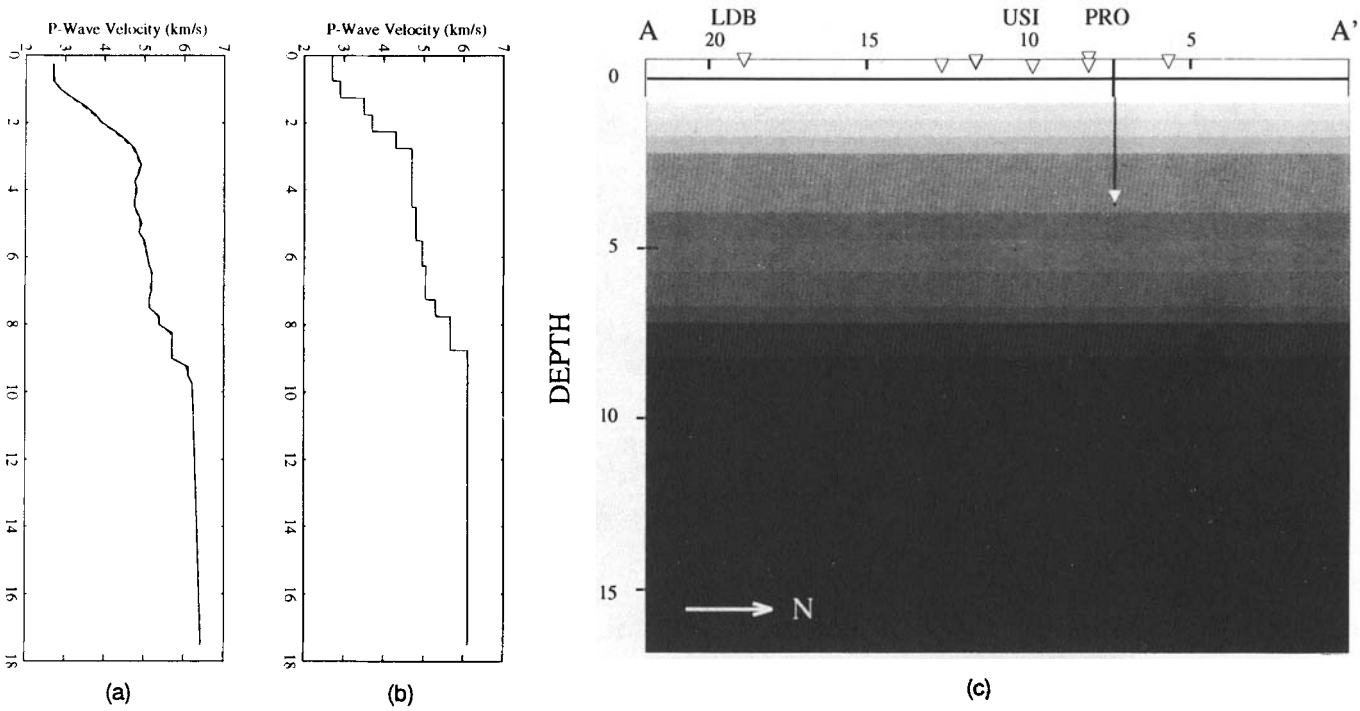


**Figure 4.** (a) Velocity versus depth graph deduced from the smoothed 3-D velocity model by averaging the velocities in each 250 m thick layer. (b) Velocity versus depth graph reduced to 12 layers deduced from (a). (c) North–south cross-section of this flat-layered model used for HYPO71 locations.

## 4 THE SEISMICITY OF THE LACQ GAS FIELD REVISITED USING THE NEW LOCATION METHOD

### 4.1 Data and errors

From the 18 years of nearly continuous seismic monitoring of the Lacq gas field, we use only the 518 earthquakes recorded by a minimum of six stations. Moreover, for this period we define two subsets of data. The first one comprises 138 events that were recorded on a borehole seismometer located in an unused gas well at a depth of 3880 m in addition to the surface stations. The second subset consists of 68 events for which a three-component record at station USI is also available. These two subsets allow us to refine the locations of the hypocentres. The advantages of using *S* phases to help constrain earthquake location have been recognized for some time (Schwartz & Nelson 1991), but data collected with borehole seismometers were only occasionally used to improve the locations.

Figure 7 shows the accuracy of the readings of both *P*- and *S*-wave arrivals. The standard deviation of the *P* and *S* readings is estimated at 0.02 s for most of the events and stations. As we do not use correlation techniques to read the arrival time, the covariance matrix $\mathbf{C}_t$ for the observations is supposed diagonal. We also need an estimation of the error made when computing the theoretical traveltimes. This error is more difficult to estimate, and may be split into several parts. (1) The main part is due to the inaccuracy of the velocity model used. This model is good in the central and shallow parts of the anticline, where the boreholes are dense, however it is more coarse in the surrounding areas and at depths greater than 6 km, for which the velocity estimate is deduced from seismic profiles only. For depth ranging from 9 to 17.5 km an average crustal velocity model is used. (2) Computational errors due to the grid ray tracing method itself are several orders of magnitude smaller than the model misfit errors. They are basically due to the discrepancy between the plane wavefront assumption and the actual curvature of the wavefront. (3) Errors due to mislocation of the recording stations are negligible in our case.

As the model misfit errors are predominant, we can no longer assume the theory covariance matrix $\mathbf{C}_T$ to be diagonal and we have to estimate its off-diagonal terms. The diagonal term of $\mathbf{C}_T$ is estimated using the equation of Pavlis (1986) which gives the upper bound for the traveltime error as the multiplication of the ray length by the maximum slowness perturbation along the ray. We take $\sigma^2 = 0.005\ \mathrm{s}^2$ corresponding to a maximum velocity error of $\pm 0.1\ \mathrm{km\ s}^{-1}$. The off-diagonal terms are computed using the equation:

$$\mathbf{C}_T^{ij} = \sigma^2 \exp\left(-\frac{d_{ij}^2}{\Delta^2}\right), \tag{4}$$

where $d_{ij}$ is the distance between the two stations $i$ and $j$ and $\Delta$ is the correlation distance of the medium chosen here equal to the dominant wavelength of 0.5 km. The off-diagonal terms remain small since the nearest stations are 2 km away. Although ray paths are close together near the source, eq. (4) does not take into account the common influence of near-source velocity misestimation.

The covariance matrices $\mathbf{C}_t$ and $\mathbf{C}_T$ play a key role in the

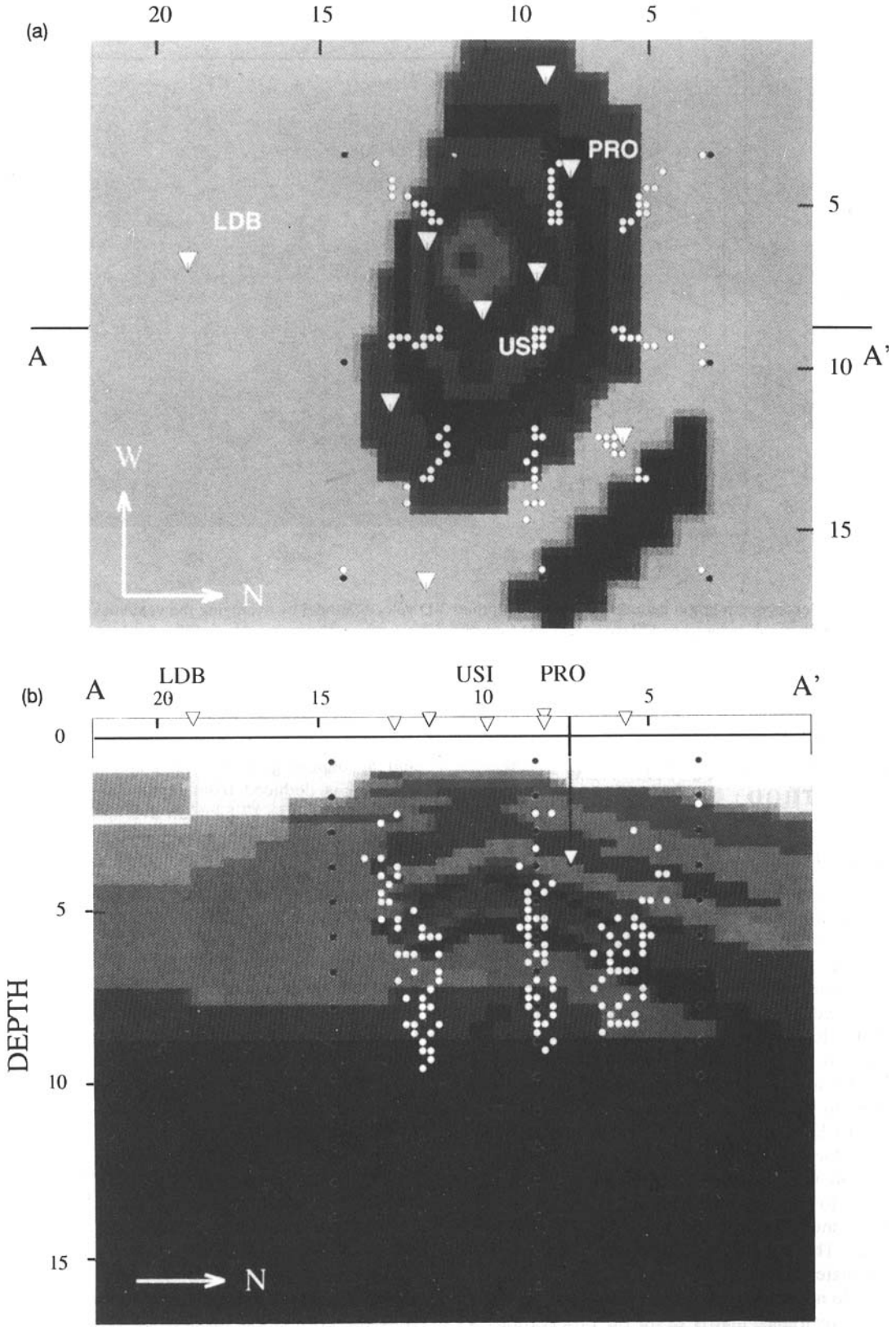


**Figure 5.** Locations obtained for the synthetic data comparing 3DGRIDLOC and HYPO71. The backgrounds for these figures are the velocity model as shown in Fig. 1. (a) HYPO71 map view. (b) HYPO71 vertical north–south cross-section. (c) 3DGRIDLOC map view. (d) 3DGRIDLOC vertical north–south cross-section.

The synthetic hypocentres (full circles) are located along nine vertical lineaments. Five of these lineaments are outside the area covered by the network. The spacing between the foci in the vertical direction is 1 km. The computed hypocentres are represented with open circles.

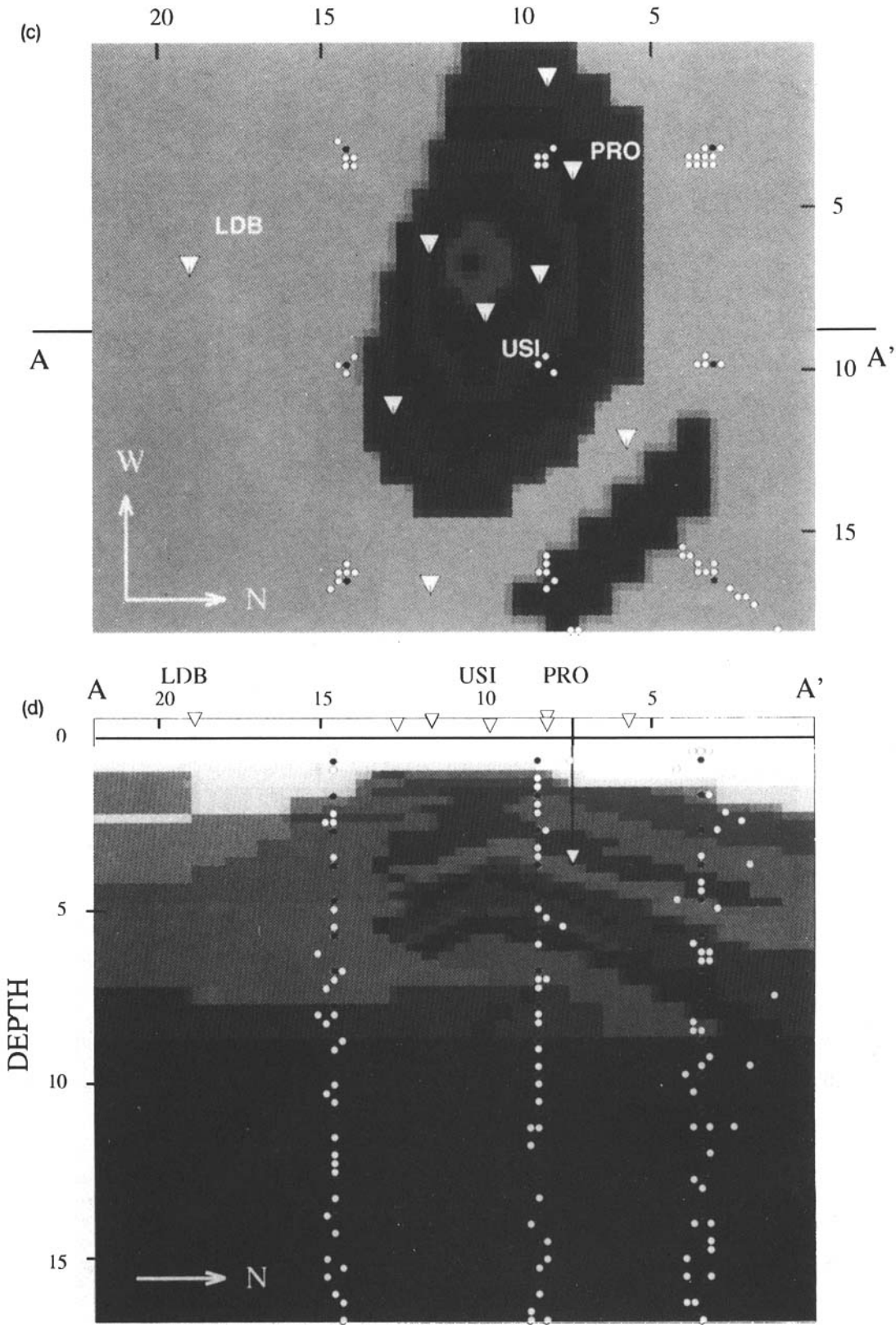


**Figure 5.** (*Continued.*)

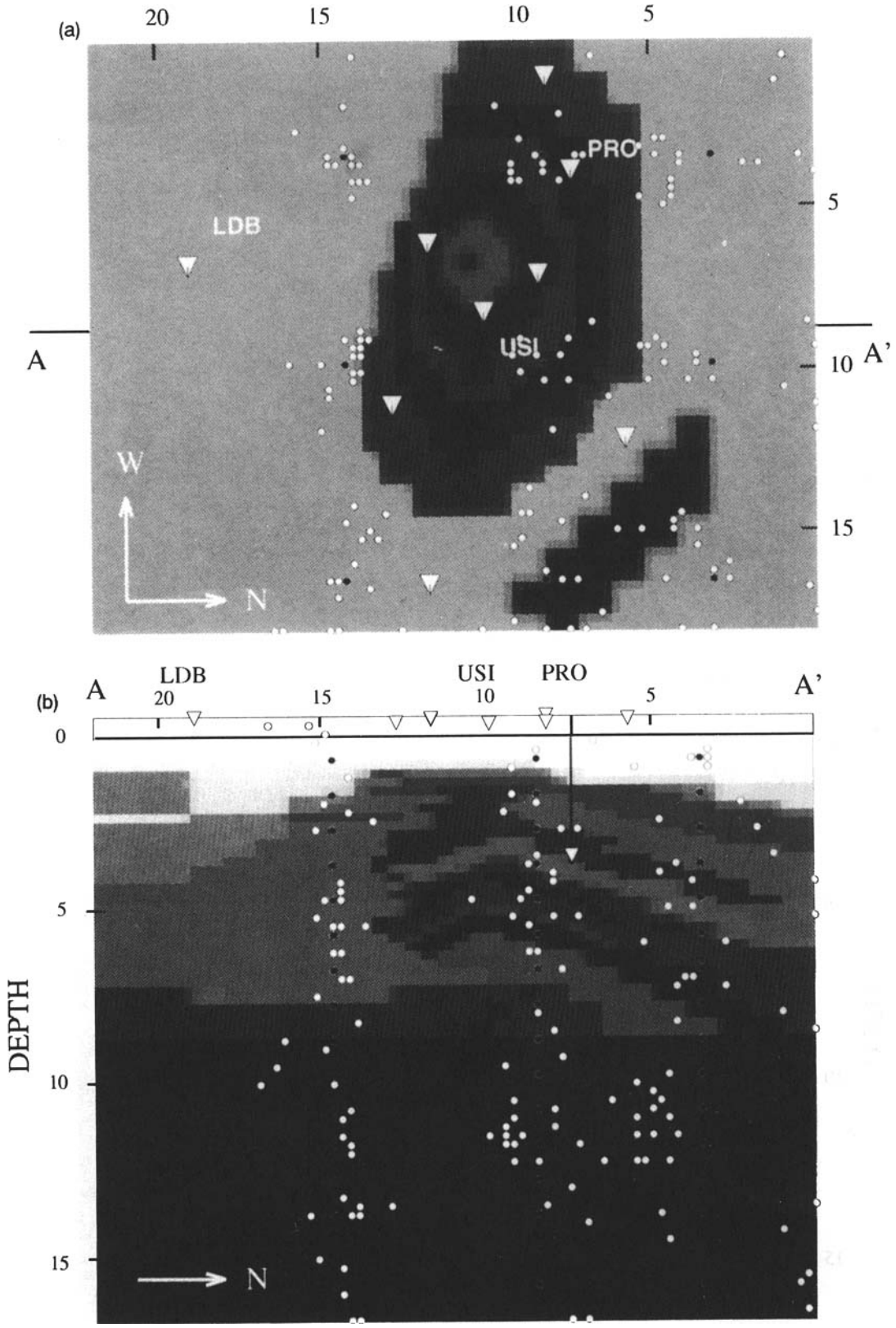


**Figure 6.** Synthetic tests for robustness of 3DGRIDLOC (a and b) and sensitivity (c and d) on map views and vertical north–south cross-sections. Synthetic foci are the same as in Fig. 5.

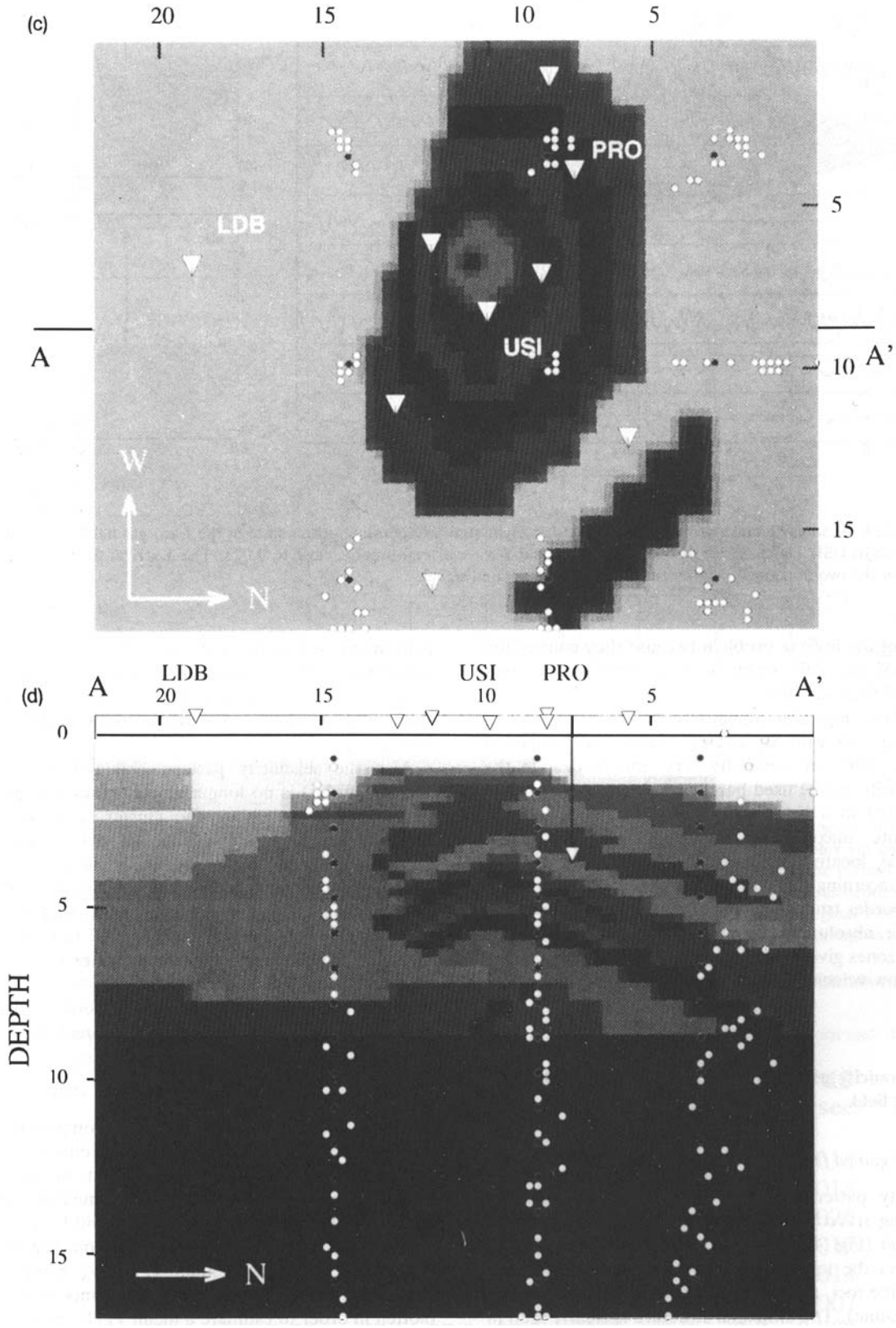


**Figure 6.** (*Continued.*)

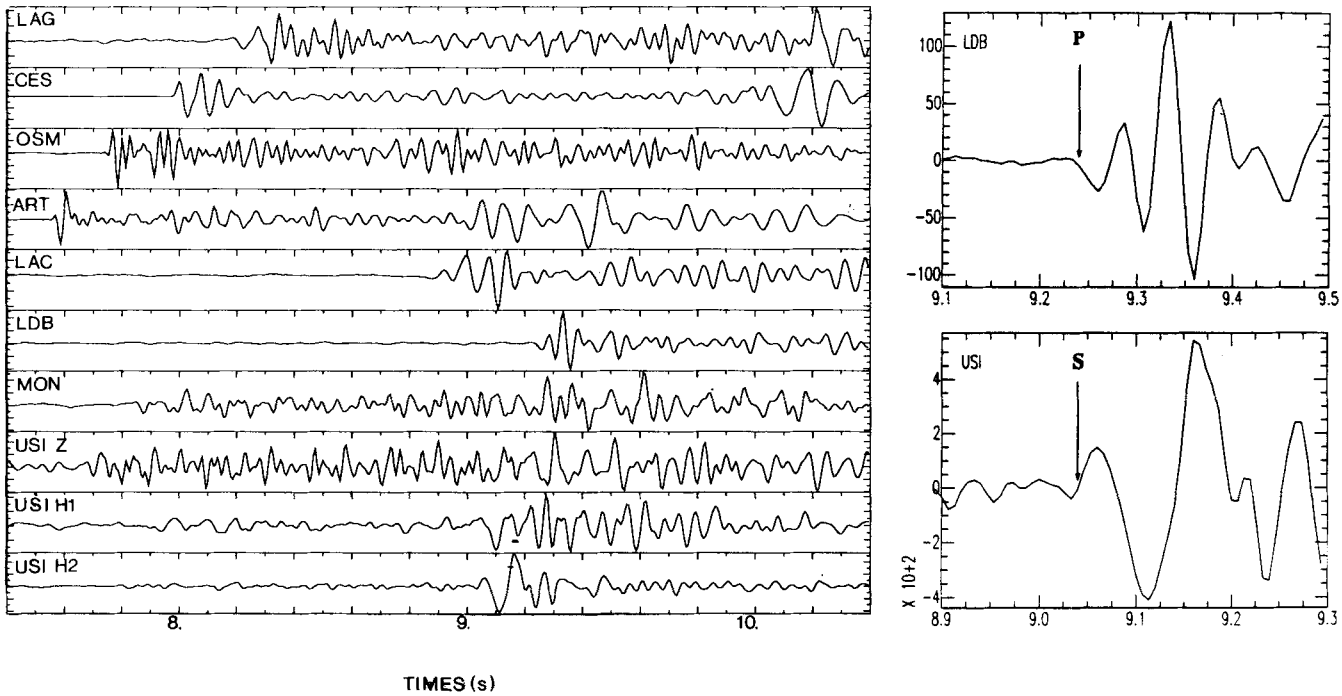


**Figure 7.** Example of an earthquake recorded in 1991 at the eight stations operating at this time in the Lacq gas field. The three-component station is located at USI. The accuracy of reading both *P*- and *S*-wave arrival times is close to 0.02 s. The *S* arrival time is taken as the mean value picked on the two horizontal components and not on a rotated signal.

formulation of the inverse problem because they control the smoothness of the PdF which in turn controls the error estimations of the locations.

Figure 8 shows typical marginal PdF obtained for the real data using eq. (1) with $\mathbf{C}_t$ and $\mathbf{C}_T$ defined as explained above. These PdFs are generally very smooth despite the complex velocity model used here, and show clear absolute maxima located in a single cell. For this reason, locating using absolute maxima of the PdF gives the same hypocentre as locating using expected value (Table 1). However, concerning the computation time and possible bias due to border truncation, in the following we choose to use only the absolute maxima location procedure. The low-velocity zones give small values for the PdF (Fig. 8) and so these low-velocity zones are unlikely hypocentre locations.

## 4.2 The seismicity pattern of the induced earthquakes of the Lacq gas field

### *4.2.1 Image gained from the whole data set*

The seismicity pattern for the 518 selected earthquakes obtained using HYPO71 and the previously defined layered velocity model (Fig. 4b), is given in Figs 9(a) and (b). As pointed out in the test example, we again observe strong clustering of the foci, mainly below the reservoir trap (marls of Sainte-Suzanne). The anticlinal structure is clearly seen in the seismicity pattern obtained by HYPO71. Detailed discussions of the seismicity pattern can be found in Grasso & Wittlinger (1991), Grasso *et al.* (1991) and Guyoton *et al.* (1992). The question arises, however, as to whether such a convenient seismicity pattern, which can so easily be connected with the geological structure is real? HYPO71 locations for synthetic data using the same velocity structure show drastic mislocations when using a layered velocity model.

Also the seismicity pattern obtained with 3DGRIDLOC (Figs 9c and d) is no longer closely related to the anticlinal structure. In particular, the clustering effect caused by shortcomings in the velocity model disappears. The 3DGRIDLOC locations are generally deeper than HYPO71 locations. A similar observation has already been reported by Nelson & Vidale (1990) for Bear Valley, California, earthquakes. We observe a general NE trend elongation of the seismicity and some deep foci cluster into a cylinder to the SE of the gas field.

In the following we have a closer look at the locations obtained from the two data subsets defined above.

### *4.2.2 Image gained from the 'S-arrival' subset*

There are data for only one three-component recording station located at USI, observing 68 events in 1991–92 and in addition we are lacking information on precise *S*-wave velocities due to the lack of *S*-wave measurements in the boreholes. The theoretical traveltime grid for the *S* waves at station USI is thus simply deduced from the *P*-wave grid multiplying it by an estimated $V_P/V_S$ ratio. Generally, Wadati diagrams using several three-component stations are plotted in order to estimate a mean $V_P/V_S$ ratio. In our case, due to a single three-component station, this technique is not applicable. The $V_P/V_S$ ratio is then deduced from a least-squares adjustment of a plot giving $(t_S-t_P)$-time versus $t_P$-traveltime at station USI, using the locations obtained

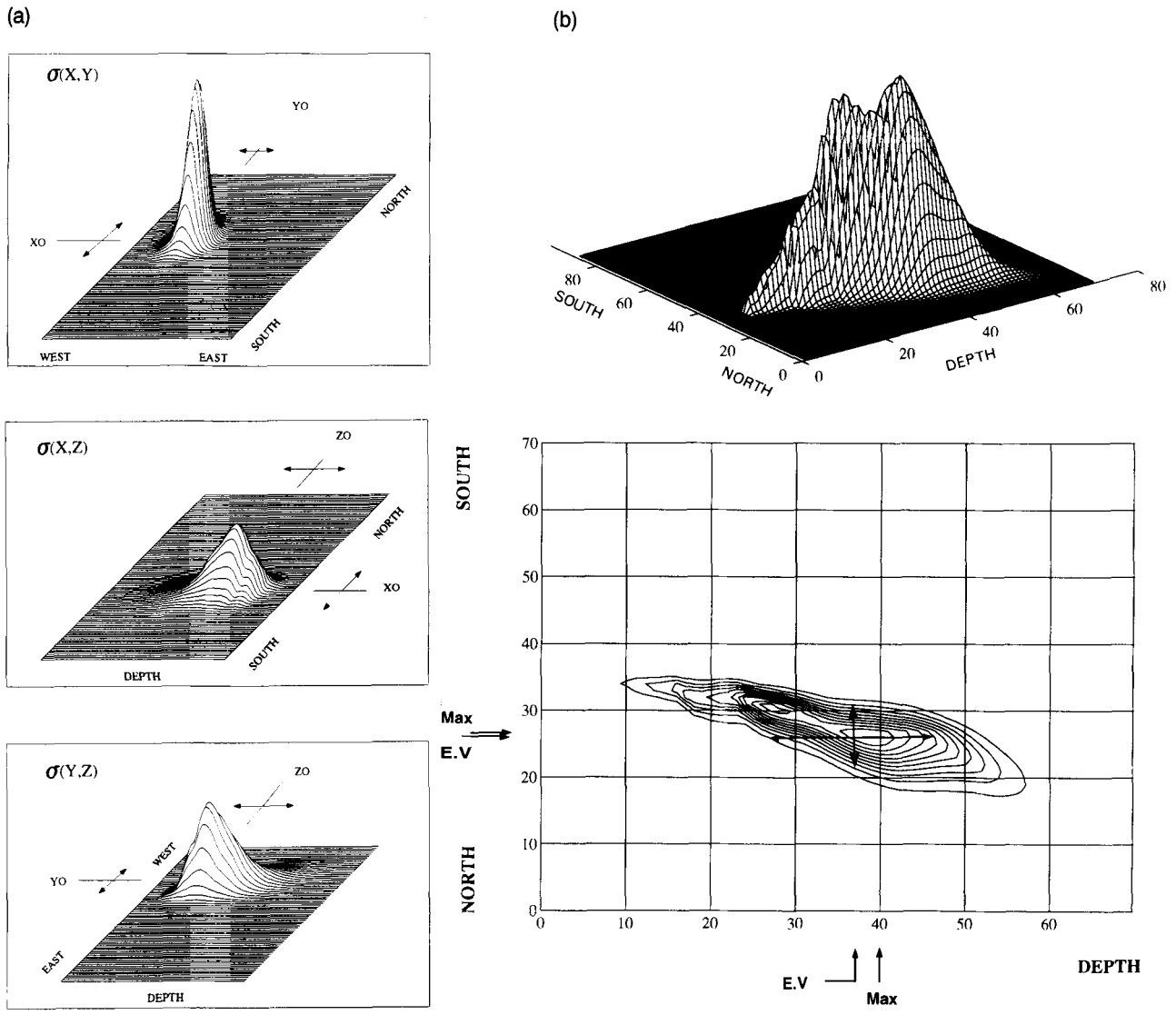


**Figure 8.** (a) An example of three marginal PdF, $\sigma(X, Y)$, $\sigma(X, Z)$ and $\sigma(Y, Z)$ obtained for an earthquake recorded at eight stations, without $S$-wave readings. $\sigma(X, Y)$, the PdF of the horizontal coordinates has a very regular shape despite the complex velocity model; this leads to a precise horizontal location using both the maximum value of $\sigma(X, Y)$ and the expected value. In contrast, the vertical cross-sections $\sigma(X, Z)$ and $\sigma(Y, Z)$ are more irregular; the effects of low-velocity zones are obvious. This leads to a more ambiguous depth determination and a possible bias between absolute maximum and expected value locations. (b) An example of an asymmetrical marginal PdF $\sigma(X, Z)$ with associated contour plot, on which we show the two possible focus determinations using the expected value (EV) or the maximum of the probability density function (Max).

The value of the standard deviations Var $(X)$, Var $(Y)$, Var $(Z)$ is a fair approximation of the mislocation and is reported on these figures $(\leftrightarrow)$.

**Table 1.** Locations of 10 events with 3DGRIDLOC using maximum value or expected value of the PdF. Locations and standard deviations are given in number of cells. NB, number of stations used.

| Date | Time | Maximum Value | | | Expected Value | | | σ(x) | σ(y) | σ(z) | RMS (sec) | NB |
|---|---|---|---|---|---|---|---|---|---|---|---|---|
| | | x | y | z | x | y | z | | | | | |
| 82 06 23 | 16 09 | 40 | 31 | 18 | 40.4 | 31.2 | 18.8 | 0.8 | 0.9 | 1.3 | 0.012 | 8 |
| 83 01 07 | 10 57 | 35 | 25 | 19 | 35.3 | 24.8 | 19.4 | 1.0 | 0.8 | 1.7 | 0.013 | 8 |
| 83 03 30 | 20 00 | 43 | 50 | 19 | 43.3 | 50.2 | 19.3 | 1.0 | 1.0 | 1.5 | 0.026 | 8 |
| 83 04 16 | 06 00 | 46 | 40 | 22 | 45.5 | 39.7 | 21.8 | 0.9 | 0.8 | 1.9 | 0.012 | 8 |
| 83 04 17 | 19 56 | 45 | 40 | 21 | 45.4 | 39.5 | 21.1 | 0.9 | 0.8 | 1.9 | 0.014 | 8 |
| 83 04 21 | 23 00 | 32 | 46 | 25 | 31.5 | 46.3 | 25.4 | 1.2 | 1.2 | 2.6 | 0.007 | 9 |
| 83 05 16 | 23 45 | 47 | 28 | 29 | 47.1 | 27.5 | 28.9 | 1.0 | 0.9 | 2.3 | 0.009 | 9 |
| 83 05 22 | 00 26 | 35 | 24 | 18 | 35.3 | 24.4 | 18.8 | 0.9 | 0.7 | 1.5 | 0.010 | 9 |
| 83 05 25 | 07 06 | 53 | 31 | 15 | 52.6 | 30.8 | 14.9 | 0.8 | 0.8 | 1.2 | 0.015 | 9 |
| 83 07 02 | 21 14 | 46 | 41 | 21 | 45.5 | 40.7 | 21.4 | 0.9 | 1.1 | 1.8 | 0.009 | 8 |

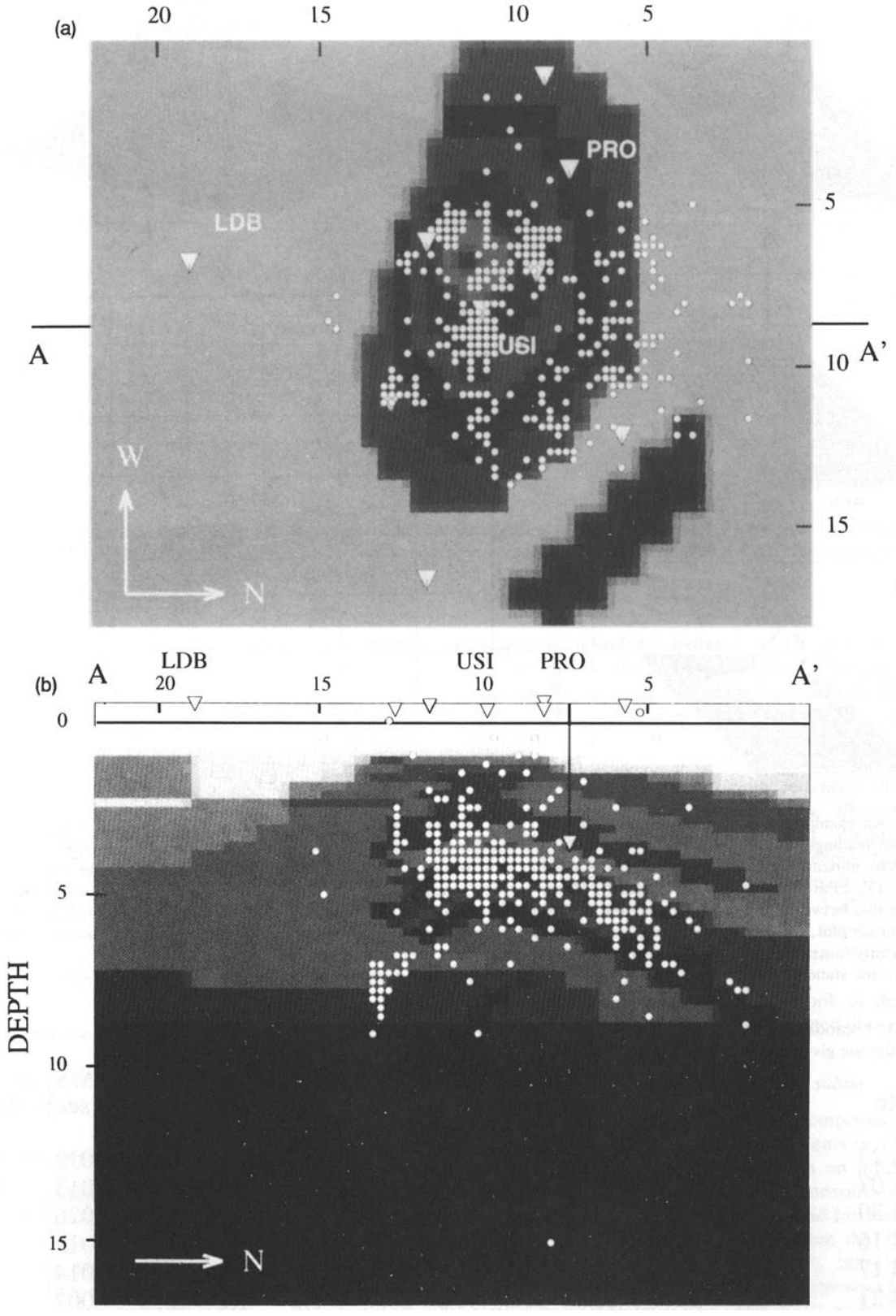


**Figure 9.** Epicentre map of the 518 relocated events from 1975 to 1992 using HYPO71 (a and b) and 3DGRIDLOC (c and d). For both methods we use only the earthquakes recorded by at least six stations. For HYPO71 locations, no station correction is applied.

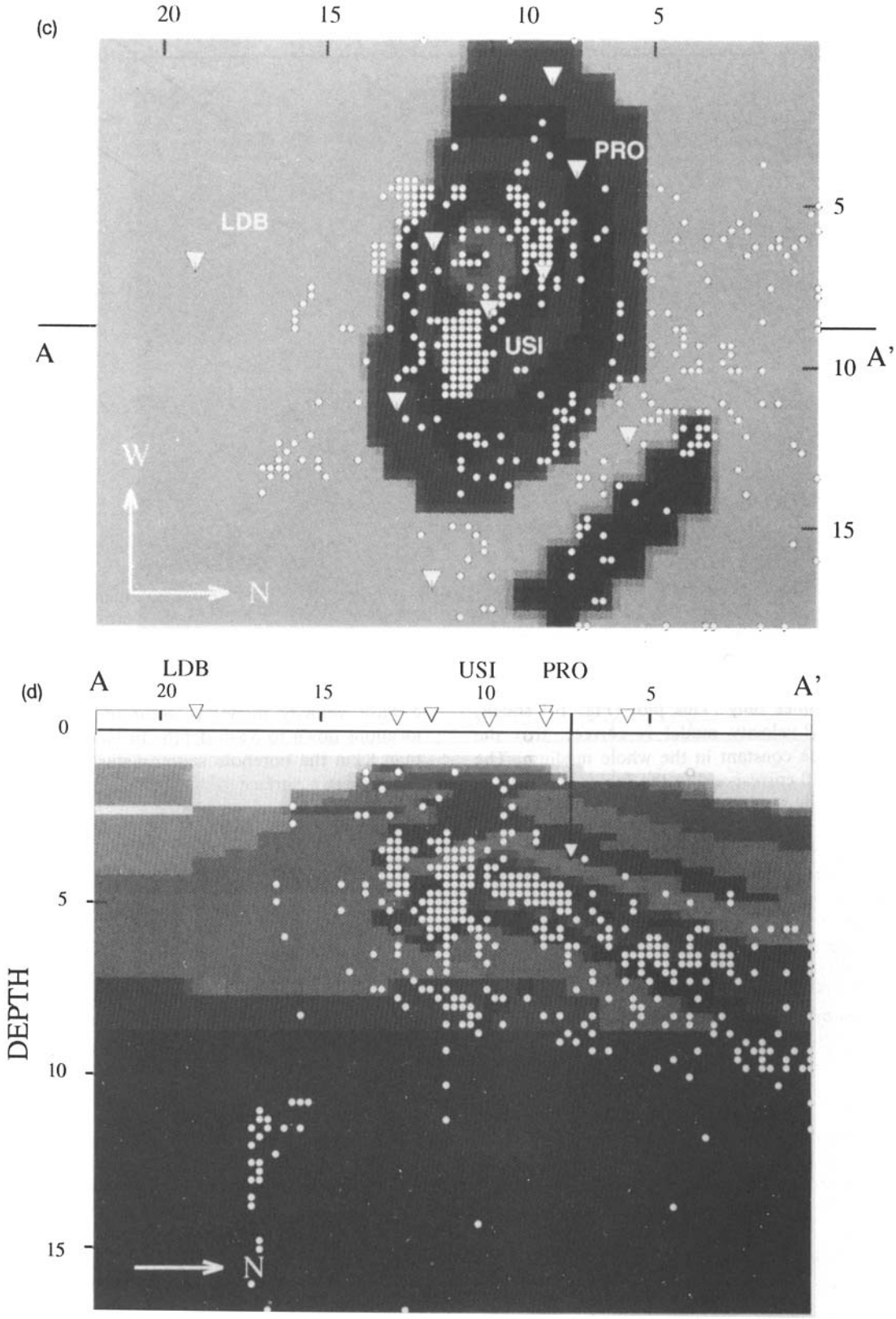


**Figure 9.** (*Continued.*)

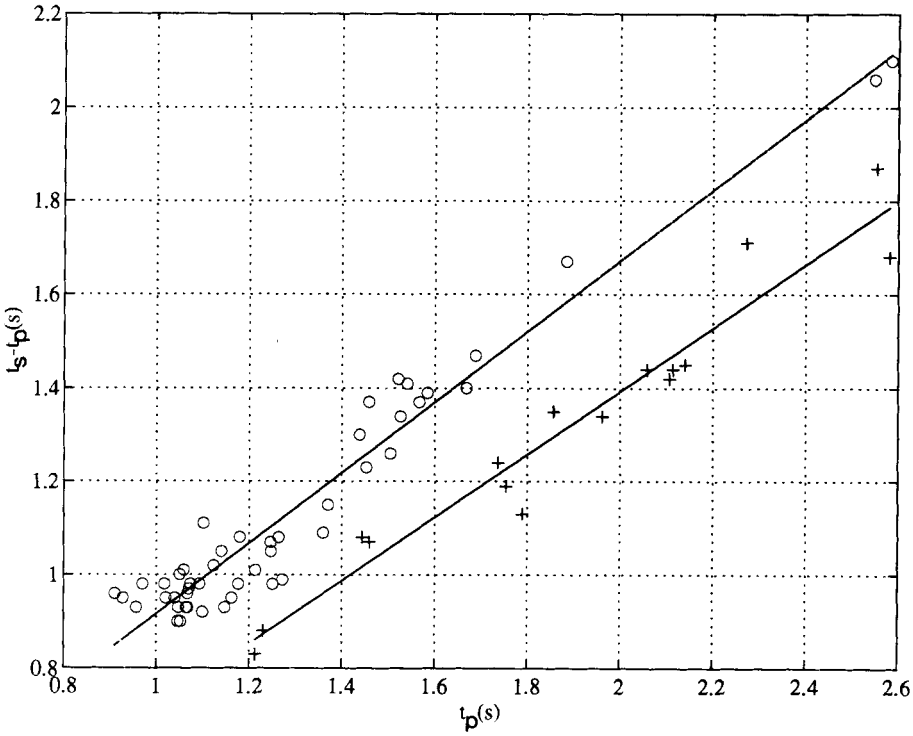


**Figure 10.** ($t_S$–$t_P$) versus $t_P$ graph for the three-component station USI. The traveltime $t_P$ is the computed traveltime (with the PL method) at station USI using the location obtained with the $P$-waves only. ($t_S$–$t_P$) are the observed differences for $S$ and $P$ arrival times at station USI: ○ correspond to the foci represented by ○ in Fig. 12 and + to the foci represented by + on the same figure. We see two families of hypocentres: one superficial, with a $V_P/V_S$ ratio of 1.76 and the other deeper one with a mean $V_P/V_S$ ratio of 1.66.

with the $P$ arrival times only. This plot (Fig. 10) shows, assuming that the $P$-velocity model is correct, that the $V_P/V_S$ ratio cannot be constant in the whole medium. The '○' symbols in Fig. 10 correspond to the foci located above 8 km depth (we use the same symbol in Fig. 11a) and having a mean $V_P/V_S$ ratio close to 1.76 while the '+' symbol corresponds to deeper foci where mean $V_P/V_S$ is close to 1.66. Such differences in mean $V_P/V_S$ ratios may be connected with the observed lithological differences existing between the upper and the lower parts of the Lacq structure (Grasso & Wittlinger 1990; Guyoton *et al.* 1992).

Inverting this subset of data using these two $V_P/V_S$ ratios for calculating the theoretical $S$ traveltimes, we obtain (Fig. 11a) locations that are close to those obtained from $P$ waves only (Fig. 11b). The discrepancy between $P$ and $P+S$ locations observed for some deep foci is probably due to the crude $V_P$ model that was used for depths greater than 10 km; for these foci only $S$ arrivals give information for correct depth determinations. Even using 3DGRILOC localization with both $P$ and $S$ waves remains important in order to obtain a good accuracy that can compensate for some deficiencies of the $P$-velocity model. The locations obtained by using $S$ waves confirm the major features of the seismicity pattern obtained from $P$ waves.

### 4.2.3 *Image gained from the 'borehole' subset*

The use of borehole seismometer data (PRO) leads to weak differences only in the seismicity pattern (Fig. 12). This is not a surprising result because at the time of operation (1982–83) the deep seismicity had not yet appeared, and the $P$-wave velocity model is accurate enough to determine locations down to 8 km depth. In fact, for events shallower than 8 km the borehole seismometer has roughly the same 'weight' as a surface station owing to the accuracy of the $P$-velocity model.

### 4.2.4 *New insight into the induced seismicity*

Earlier locations of this induced seismicity were performed using several different localization methods: the first to mention was HYPO71 (Wittlinger 1980). Later came an approach that simultaneously inverted for focal parameters and velocity (Grasso & Wittlinger 1990) and finally Roecker's (1982) method, using a 3-D model (Guyoton *et al.* 1992) was adopted. The seismicity patterns obtained with these methods are never very different from each other but provide more and more detail leading to convincing interpretation. Strong correlation of seismicity patterns with the geological structure can be seen for all of their locations, but only the last one using a 3-D model shows the existence of a deep seismicity (up to 10 km depth) and that most of the earthquakes are located beneath the gas reservoir.

The 3DGRIDLOC method discussed in this paper provides new details, showing a spread-out pattern of seismicity: not all of the foci seem to cluster in the vicinity of the central part of the reservoir. Induced seismicity may occur as far as 10 km from the reservoir and involves a greater volume than expected from the earlier locations. Clearly the foci are always located deeper than the impermeable layer trapping the reservoir and even deeper than the reservoir itself. Some deep foci occur along postulated tectonic faults at up to

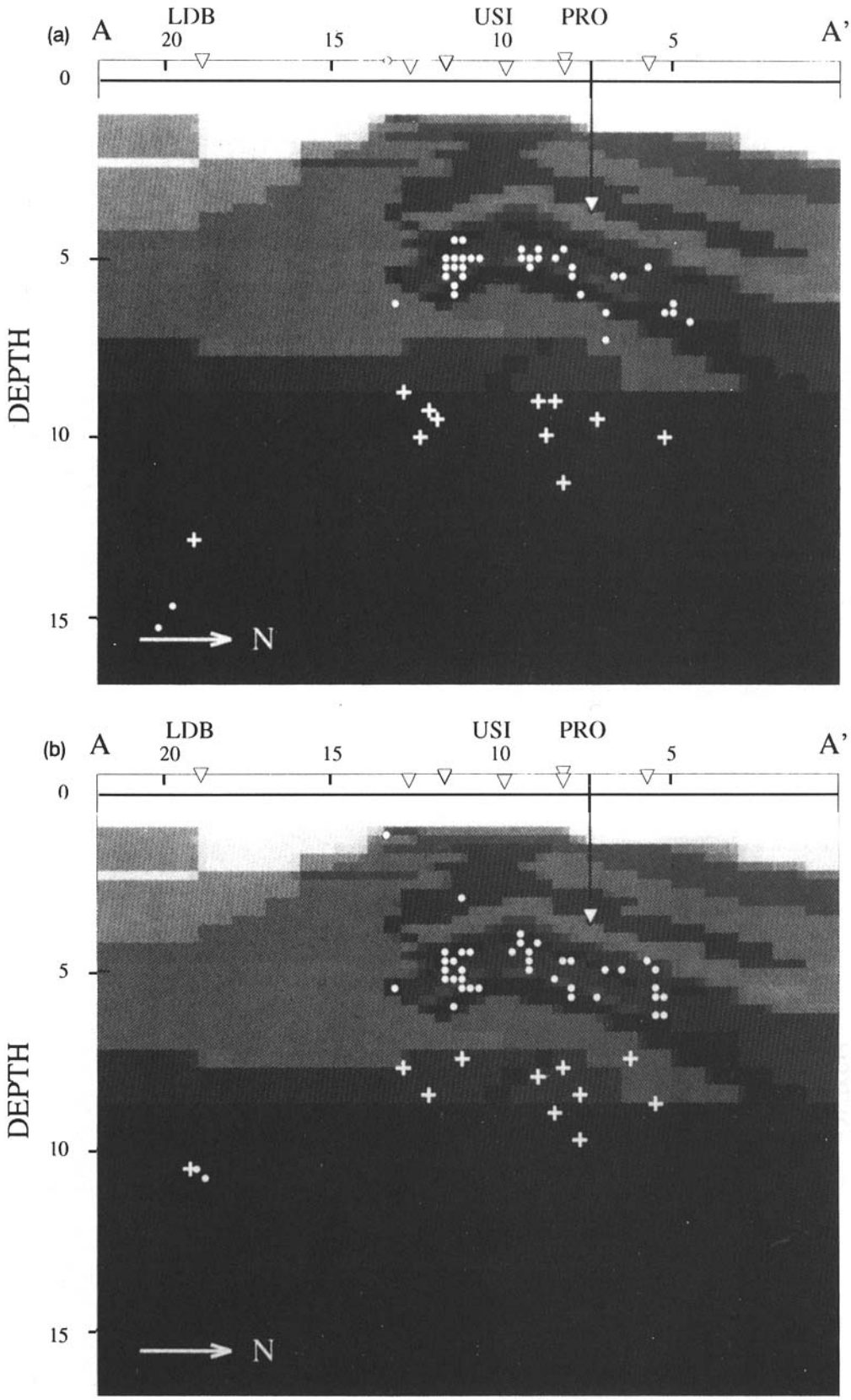


**Figure 11.** Comparative locations during 1991–92 using (a) and not using (b) *S* waves recorded at station USI. The $V_P/V_S$ ratios that we use are deduced from Fig. 10: 1.76 up to 8 km depth and 1.66 for greater depths. The hypocentres corresponding to the symbols + are always deeper than the hypocentres represented by ○ corresponding to the area of coarse $V_P$ velocity model.

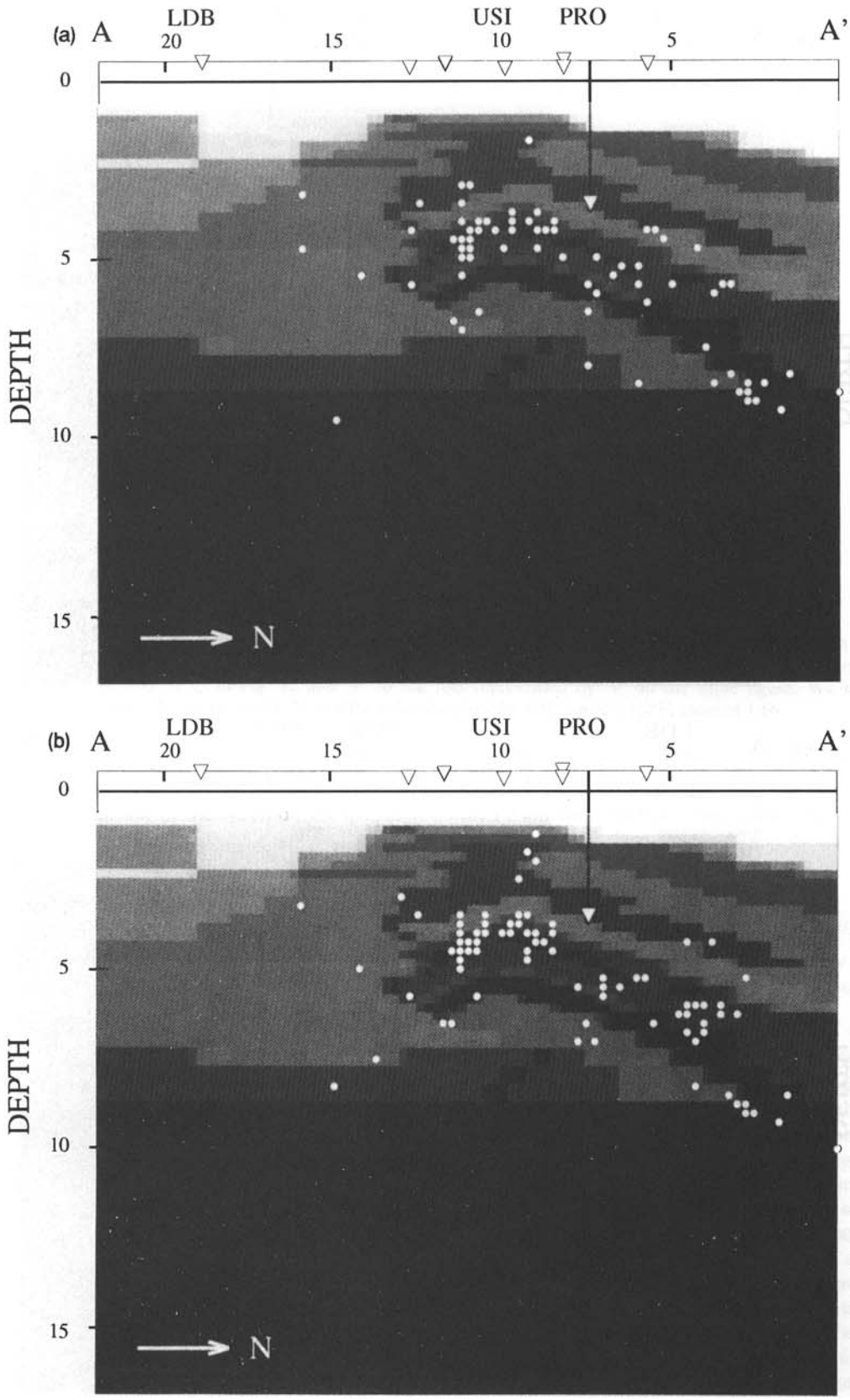


**Figure 12.** Comparative locations during 1982–83 using (a) and not using (b) borehole seismometer data at station PRO. Owing to the good velocity model for the upper 8 km, the use of this borehole station does not greatly change the pattern of seismicity. Thus, if we use a reliable velocity model and a proper location method the operation of expensive borehole instruments is less useful than three-component stations.

18 km depth, largely deeper than the sedimentary cover. Careful observation of the seismicity pattern also shows that the foci concentrate in high-velocity zones. This does not seem to be an artefact of the method since the synthetic test does not show such a distinctive feature. Excepting the deep foci located in the basement in the SE part of the gas field, which appeared after 1982, there is no obvious depth migration of the hypocentres during all the observation period.

## CONCLUSIONS

This paper shows that a proper location method using a velocity model as close as possible to the real one, gives new insight into the interpretation of seismicity patterns. The method we propose is characterized by the use of expended finite differences for traveltime computations and a probability density function for the hypocentre localization. 3DGRIDLOC is adequate to use complex 3-D velocity models for *P* and *S* waves.

3DGRIDLOC is robust with respect to arrival time reading errors and insensitive to weak variations in the velocity model as shown for a synthetic and a real data set example. The probability density function allows an easy estimation of the localization errors and their quality.

Comparison with older methods, as for the case of subduction zones, indicates that this method should be used to restudy the seismicity patterns for other structurally complex areas.

## ACKNOWLEDGMENTS

We thank P. Podvin and I. Lecomte for their code to compute traveltimes in three dimensions and for helpful advice, F. Guyoton and J. R. Grasso for the initial 3-D velocity model of the Lacq gas field and M. Frogneux for the arrival times used in the example given. We have benefited from numerous and pertinent discussions with J. J. Leveque, L. Rivera and U. Achauer. J. J. Leveque and J. Helm critically reviewed an earlier version of this paper. We acknowledge the constructive review of J. E. Vidale. The authors thank the Société Nationale Elf-Aquitaine for sponsoring the seismic monitoring of the Lacq gas field.

## REFERENCES

Babuska, V. & Cara, M., 1991. *Seismic Anisotropy in the Earth, Modern Approaches in Geophysics,* Vol. **10,** Kluwer Academic Publishers, Dordrecht.

Geiger, L., 1912. Probability method for the determination of earthquake epicenters from the arrival time only, *Bull. St Louis Univ.,* **8,** 60–71.

Grasso, J. R. & Wittlinger, G., 1990. Ten years of seismic monitoring over a gas field, *Bull. seism. Soc. Am.,* **80,** 450–473.

Grasso, J. R., Volant, P., Fourmaintraux, D. & Maury, V., 1991. Relation between hydrocarbon extraction, local triggered earthquakes and major regional earthquakes: example of the Pyrenean area, in *32nd U.S. Symposium on Rock Mechanics, Oklahoma,* 1991.

Guyoton, F., Grasso, J. R. & Volant, P., 1992. Interrelation between induced seismic instabilities and complex geological structure, *Geophys. Res. Lett.,* **19**(7), 705–708.

Hirata, N. & Matsu'ura, M., 1987. Maximum-likelihood estimation of hypocenter with origin time elimination using nonlinear inversion technique, *Phys. Earth planet. Inter.,* **47,** 50–61.

Lecomte, I., 1992. Analysis of finite-difference calculations of traveltimes, *Report, NTNF/NORSAR,* Kjeller, Norway.

Lecomte, I., 1993. Finite-difference calculations of first traveltimes in anisotropic media, *Geophys. J. Int.,* **113,** 318–342.

Lee, W. H. K. & Lahr, J. C. 1975. HYPO71 (revised): a computer program for determining hypocenter, magnitude and first pattern of local earthquakes, *US Geol. Surv. Open-File Rep.* **75-311,** 1–116.

Moser, T. J., 1991. Shortest path calculation of seismic rays, *Geophysics,* **56,** 59–67.

Moser, T. J., Van Eck, T. & Nolet, G., 1992. Hypocenter determination in strongly heterogeneous earth models using the shortest path method, *J. geophys. Res.,* **97,** 6563–6572.

Nelson, G. D. & Vidale, J. E., 1990. Earthquake locations by 3D finite-difference travel times, *Bull. seism. Soc. Am.,* **80,** 395–410.

Pavlis, G. L., 1986. Appraising earthquake hypocenter location errors: a complete practical approach for single-event locations, *Bull. seism. Soc. Am.,* **76,** 1699–1717.

Podvin, P. & Lecomte, I., 1991. Finite difference computation of traveltimes in very contrasted velocity models: a massively parallel approach and its associated tools, *Geophys. J. Int.,* **105,** 271–284.

Roecker, S. W., 1982. Velocity structure of the Pamir–Hindu Kush region: possible subducted crust, *J. geophys. Res.,* **87,** 945–959.

Schwartz, S. Y. & Nelson, G. D., 1991. Loma Prieta aftershock relocation with S–P traveltimes: effects of 3 D structure and true error estimates, *Bull. seism. Soc. Am.,* **81,** 1705–1725.

Tarantola, A. & Valette, B., 1982. Inverse problems = quest for information, *J. Geophys.,* **50,** 159–170.

Vidale, J. E., 1988. Finite-difference calculation of travel times, *Bull. seism. Soc. Am.,* **78,** 2062–2076.

Vidale, J. E., 1990. Finite-difference calculation of travel times in 3D, *Geophysics,* **55,** 521–526.

Wittlinger, G., 1980. Etude de la sismicité en champ proche par un réseau sismologique à faible ouverture: application au Frioul (Italie) et au gisement de Lacq (France), *Thèse de Doctorat d'Etat,* University of Strasbourg, France.